Analysis of one-proton transfer reaction in $^{18}O + ^{76}Se$ collisions at 275 MeV

I. Ciraldo,[1,2,*] F. Cappuzzello,[1,2] M. Cavallaro,[1] D. Carbone,[1] A. Gargano,[3] G. De Gregorio,[3,4] H. Garcia-Tecocoatzi,[5] E. Santopinto,[5] R. I. Magaña-Vsevolodovna,[5,6] L. Acosta,[7] C. Agodi,[1] P. Amador-Valenzuela,[8] G. A. Brischetto,[1,2] S. Burrello,[1] D. Calvo,[9] E. R. Chávez Lomeli,[7] M. Colonna,[1,2] F. Delaunay,[1,2,10] H. Djapo,[11] C. Eke,[12] P. Finocchiaro,[1] S. Firat,[13] M. Fisichella,[1] M. A. Guazzelli,[14] A. Hacisalihoglu,[15] R. Linares,[16] N. H. Medina,[17] M. Moralles,[18] J. R. B. Oliveira,[17] A. Pakou,[19] L. Pandola,[1] H. Petrascu,[20] F. Pinna,[9,21] O. Sgouros,[1,2] S. O. Solakci,[13] V. Soukeras,[1,2] G. Souliotis,[22] A. Spatafora,[1,2] D. Torresi,[1] S. Tudisco,[1] A. Yildirim,[13] and V. A. B. Zagatto[16]
(NUMEN collaboration)

[1]*Istituto Nazionale di Fisica Nucleare, Laboratori Nazionali del Sud, Catania, Italy*
[2]*Dipartimento di Fisica e Astronomia "Ettore Majorana", Università di Catania, Catania, Italy*
[3]*INFN, Sezione di Napoli, Napoli, Italy*
[4]*Dipartimento di Matematica e Fisica, Università della Campania "Luigi Vanvitelli", Caserta, Italy*
[5]*INFN, Sezione di Genova, Genova, Italy*
[6]*IBM Client Innovation Center Milano, Milan, Italy*
[7]*Instituto de Física, Universidad Nacional Autónoma de México, Mexico City, Mexico*
[8]*Departamento de Aceleradores y Estudio de Materiales, Instituto Nacional de Investigaciones Nucleares, Ocoyoacac, México*
[9]*Istituto Nazionale di Fisica Nucleare, Sezione di Torino, Italy*
[10]*Université de Caen Normandie, ENSICAEN, CNRS/IN2P3, LPC Caen UMR6534, F-14000 Caen, France*
[11]*Institute of Accelerator Technologies, Ankara University, Ankara, Turkey*
[12]*Department of Mathematics and Science Education, Faculty of Education, Akdeniz University, Antalya, Turkey*
[13]*Department of Physics, Akdeniz University, Antalya, Turkey*
[14]*Centro Universitario FEI, Sao Bernardo do Campo, Brazil*
[15]*Department of Physics, Recep Tayyip Erdogan University, Rize, Turkey*
[16]*Instituto de Fisica, Universidade Federal Fluminense, Niteroi, Brazil*
[17]*Instituto de Fisica, Universidade de Sao Paulo, Sao Paulo, Brazil*
[18]*Instituto de Pesquisas Energeticas e Nucleares IPEN/CNEN, Sao Paulo, Brazil*
[19]*Department of Physics and HINP, University of Ioannina, Ioannina, Greece*
[20]*IFIN-HH, Magurele, Romania*
[21]*DISAT, Politecnico di Torino, Italy*
[22]*Department of Chemistry and HINP, National and Kapodistrian University of Athens, Athens, Greece*

(Received 19 July 2023; revised 8 November 2023; accepted 9 January 2024; published 22 February 2024)

Background: A systematic exploration of one-nucleon transfer reactions induced by the (^{18}O, ^{19}F) and (^{18}O, ^{17}O) reactions on different targets (^{12}C, ^{16}O, ^{27}Al, ^{40}Ca, ^{48}Ti, ^{76}Se, ^{116}Sn) is being performed at the Istituto Nazionale di Fisica Nucleare–Laboratori Nazionali del Sud (INFN-LNS) at beam energies higher than Coulomb barrier. A featured aspect is the adoption of a multichannel reaction approach, where several quasielastic processes are studied consistently from both the experiment and theory sides. Resembling the case of light-ion induced direct reactions, for which a large amount of data exists, the multichannel heavy-ion direct reaction is a powerful tool to characterize nuclear mean field as well as few-nucleon correlations in low-lying nuclear states. In this view, the study of different reaction mechanisms and nuclear structure models helps to characterize the nuclear wave functions and accurately scrutinize the parameters that control the uncertainties in the calculations of nuclear matrix elements (NMEs). In this context, special attention is recently paid to NMEs involved in second-order isotensor processes such as double charge exchange (DCE) and neutrinoless double beta ($0\nu\beta\beta$) decay.

Purpose: We perform the experiment and the data analysis based on theoretical models of one-nucleon transfer reactions induced by the $^{18}O + ^{76}Se$ collision at energies above the Coulomb barrier in a multichannel approach. The ^{76}Se nucleus attracts nowadays much interest since it is the daughter in the ^{76}Ge $\beta\beta$ decay, and the nuclear matrix elements involved in the $^{76}Se_{g.s.} \rightarrow {}^{76}Ge_{g.s.}$ and $^{76}Ge_{g.s.} \rightarrow {}^{76}Se_{g.s.}$ transitions are the same for time reversal symmetry. In particular, we intend to analyze transitions to low-lying excited states of the residual and ejectile nuclei in the ^{76}Se(^{18}O, ^{19}F)^{75}As one-proton pickup reaction at 275 MeV incident energy by measuring

*ciraldo@lns.infn.it

the cross section. An additional goal is to determine the role of the coupling channels in the measured cross sections, testing different model descriptions of the involved nuclear states.

Methods: Nuclear reactions induced by the $^{18}O + ^{76}Se$ collision were measured at INFN-LNS using the MAGNEX large acceptance magnetic spectrometer for the detection of the ejectiles. The missing mass technique was used for the reconstruction of the reaction kinematics. The excitation energy spectrum and the differential cross section angular distributions were the key extracted observables. The experimental data were compared with theoretical calculations based on the distorted wave Born approximation, the coupled-channels Born approximation, and coupled reaction channels. The adopted spectroscopic amplitudes for the projectile and target overlaps were derived by large-scale shell-model and interacting boson-fermion model calculations. In the calculations the initial state interaction and the nuclear structure model inputs were the same as those adopted in the study of elastic and inelastic scattering and (^{18}O, ^{17}O) one-neutron stripping reaction, published elsewhere.

Results: Peaks in the cross section energy spectra corresponding to groups of transitions to ^{75}As and ^{19}F were identified and the experimental angular distributions were compared with theoretical calculations. A fair agreement between theory and experiment both in cross section values and diffraction pattern is obtained, without the need for any scaling factor, validating the adopted reaction and nuclear structure approaches.

Conclusions: Resembling the case of the (^{18}O, ^{17}O) one-neutron stripping reaction, the couplings to the inelastic channels of projectile and target are significant for the one-proton pickup reaction and are likely to also play a role in the single and double charge exchange reactions. The fair description of the data is remarkable since no free parameter was used for this analysis, highlighting that the multichannel approach guarantees an accurate investigation of all the interesting reactions induced by the $^{18}O + ^{76}Se$ collision.

DOI: 10.1103/PhysRevC.109.024615

I. INTRODUCTION

Nowadays, outstanding experimental activity is ongoing to observe the neutrinoless double beta ($0\nu\beta\beta$) decay [1–3] for the first time. This process is potentially the best resource to probe if the neutrino and antineutrino are the same particle, one of the most important open questions of modern physics. In the description of the $0\nu\beta\beta$ decay one of the main sources of uncertainties is due to the nuclear matrix elements (NMEs)—entering the expression of the lifetime of the $0\nu\beta\beta$ decay—which are calculated adopting different theoretical nuclear structure models [4]. To date, different calculations of NMEs provide results differing up to a factor 2 or 3 among them.

In this context, the NUMEN (NUclear Matrix Elements for Neutrinoless double beta decay) project [5] aims at accessing information about the NME of neutrinoless double beta decay through an innovative technique. This is based on the measurement of the heavy-ion induced double charge exchange (HI-DCE) reaction cross sections on targets made of various $0\nu\beta\beta$ decay candidates. HI-DCE reactions are nuclear processes showing interesting analogies with $0\nu\beta\beta$ decay, in particular the initial and final nuclear states involved are the same [6–9].

In DCE reactions, as well as in all direct reactions, the cross sections critically depend on the ion-ion initial and final state interaction, which in leading order (optical model) determines the cross section for elastic scattering. In addition, the nuclear structure inputs significantly impact on the estimation of the reaction cross sections. Also, the coupling of different reaction channels could play an important role for accurate studies of the reaction cross sections and should be studied in detail. The coupling between a specific direct reaction channel with the elastic and other quasielastic processes makes it necessary to study such processes in a common approach, where different reaction channels are explored at the same time and the data are consistently analyzed. A multichannel approach [10–12] was recently proposed to explore the complete network of nuclear reaction data and extract information on the relevant ingredients involved in DCE reactions. The implementation of the multichannel approach for the study of heavy-ion induced reactions shows a wide degree of complexity from both the experimental and theoretical points of view. Experimentally, different reaction cross sections should be measured under the same laboratory conditions. Theoretically, a high degree of consistency is required in order to simultaneously treat the different degrees of freedom selectively activated by the various direct reactions within a common framework.

Moreover, the simultaneous measurement of different proton and neutron transfer channels is essential to study the involved DCE reaction mechanism. In fact, recent works suggest that DCE processes might be a combination of three different kinds of reaction dynamics sharing the same initial and final states [8,13]: the Majorana double charge exchange (MDCE), the double single charge exchange (DSCE), and the sequential multinucleon transfer (TDCE). The first two mechanisms are characterized by the exchange of charged isovector mesons, typical of nucleon-nucleon interaction. They probe the nuclear response to rank-2 isotensor operators, thus being in principle connected to $0\nu\beta\beta$ and $2\nu\beta\beta$ decays, respectively [7–9,13]. On the other hand, TDCE consists of the successive transfer of nucleons between the projectile and the target. It is triggered by the mean field action of the colliding nuclei, which does not play a role in double beta decay. Thus, TDCE represents an unwanted competing mechanism that needs to be precisely evaluated in DCE data analyses.

Recently, studies of specific systems have shown that the TDCE contribution to DCE cross section is negligible in the $^{116}Cd(^{20}Ne, ^{20}O)^{116}Sn$ reaction at 306 MeV incident energy [13,14] and in the $^{40}Ca(^{18}O, ^{18}Ne)^{40}Ar$ reaction at 270 MeV incident energy [6]. However, a critical dependence of transfer yields on kinematical conditions and on structure and multipolarities of the reacting nuclei was discussed in previous works

[11,15]. As a result, only a fully comprehensive study of heavy-ion induced transfer reactions may allow one to assess which model space, configurations, orbitals, and correlations have to be included in a nuclear structure model capable of describing experimental data.

In this view, the study of different reaction mechanisms and nuclear structure models gives important data-driven constraints on the nuclear wave functions, which are helpful for characterizing *a priori* the "ingredients" that can reduce uncertainties in the direct calculations of $0\nu\beta\beta$ decay NMEs. In this context, the experimental and theoretical analysis of one- and two-nucleon transfer reactions induced by the $^{18}O + ^{76}Se$ collision at energies above the Coulomb barrier is particularly relevant, since the ^{76}Se nucleus is the daughter in the ^{76}Ge $\beta\beta$ decay and the NMEs related to the $^{76}Se_{g.s.} \rightarrow {}^{76}Ge_{g.s.}$ and $^{76}Ge_{g.s.} \rightarrow {}^{76}Se_{g.s.}$ transitions are the same for time reversal symmetry.

In the past, heavy-ion direct transfer reactions at energies above the Coulomb barrier have been widely investigated [15–25]. A common feature in reported studies is the use of large arbitrary scaling factors in the calculated cross sections in order to reproduce experimental data. Nowadays, substantial progress in the computational and numerical sciences has opened new opportunities to adopt heavy-ion transfer reactions as tools to investigate the nuclear structure and the reaction mechanisms [12,26–31]. In this perspective, different systems have been systematically studied at the Istituto Nazionale di Fisica Nucleare–Laboratori Nazionali del Sud (INFN-LNS) (Italy) by the (^{18}O, ^{17}O), (^{18}O, ^{19}F) and (^{18}O, ^{16}O) reactions at incident energies ranging from 84 to 275 MeV [10,26–30,32–39]. Thanks to the MAGNEX large acceptance magnetic spectrometer [40,41], used to detect the ejectiles, many nuclear systems were explored, yielding high quality inclusive spectra. In this framework, the ^{18}O beam has been demonstrated to be an interesting tool to probe neutron-neutron pairing correlation in target nuclei [26,27,30,32,42–45].

In Fig. 1 the network of the nuclear reactions explored in the multichannel study of the system $^{18}O + ^{76}Se$ is shown. The analysis of the elastic, inelastic, and one-neutron stripping reactions was recently completed [37,46]. Experimentally, the reaction cross sections were measured under the same experimental conditions. The same optical potential and nuclear structure model were adopted to guarantee the reaction calculations consistency. As a result, the coupling with the inelastic channel feeding states in entrance and exit partitions was found to be important and should be accounted for in the analyses of other direct reactions such as single and double charge exchange processes involving the ^{76}Se isotope.

Very recent studies on light systems underline the importance of the coupled-channels calculations in studying nucleon transfer reactions [47–49]. Keeley *et al.* [47] confirmed that a relatively complete coupled reaction channel (CRC) calculation, including multistep reaction paths in a consistent way, should be used for a reliable extraction of the asymptotic normalization coefficients for astrophysics from heavy-ion reaction data. In addition, Wamers *et al.* [48] highlighted that effects of target excitations are important in proton knock-out reactions from ^{17}Ne at 500 MeV/u incident energy,

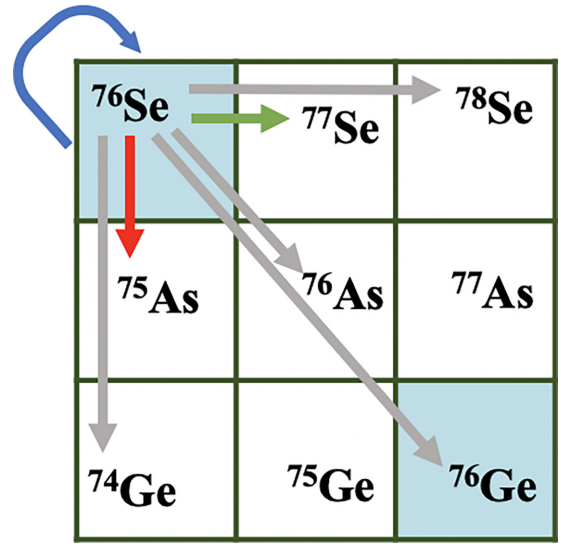

FIG. 1. Network of the nuclear reactions explored in the multichannel study of the system $^{18}O + ^{76}Se$. The elastic, inelastic, one-neutron stripping, and one-proton pickup reactions are indicated with blue, green, and red arrows. The analysis of the other reaction channels (single and double charge exchange, two-proton and two-neutron transfer in grey arrows) is under way.

arguing that the interaction between nucleons in the beam and target can perturb the reliability of structure information. Pohl *et al.* [49] concluded that multiple reaction mechanisms, including the quasifree knockout, inelastic scattering, and nucleon transfer processes, should be considered in analyses of inclusive one-nucleon removal cross sections measured at intermediate energies for quantitative investigation of single-particle strengths and correlations in atomic nuclei.

The experimental and theoretical study of the $^{76}Se(^{18}O, ^{19}F)^{75}As$ reaction at 275 MeV incident energy is presented here for the first time. This work is a part of a systematic study at INFN-LNS aiming to investigate a network of reactions within the NUMEN and NURE [50] projects, with the final goal of studying the $^{76}Se(^{18}O, ^{18}Ne)^{76}Ge$ DCE reaction. The explorations of the ^{76}Se and ^{76}Ge targets are highly complementary, allowing a detailed characterization of the parent and daughter systems of the ^{76}Ge $\beta\beta$ emitter. The multiparametric experimental data reduction together with advanced theoretical calculations allow an accurate analysis of the transfer reaction channels. In particular, excitation energy spectra are shown together with cross section angular distributions for the transitions to the ground and low-lying excited states. The spectroscopic amplitudes for the projectile and target overlaps are obtained from large-scale shell-model and interacting boson-fermion model calculations. Nuclear reaction calculations are performed to an increasing level of sophistication, adopting the distorted wave Born approximation (DWBA), the coupled-channels Born approximation (CCBA), and coupled reaction channel (CRC) approaches [13].

The paper is organized as follows. Sec. II describes the experimental setup and the data reduction technique. In Sec. III the theoretical approaches used in the data analysis and the

comparison of the calculations with the experimental data are presented. The obtained results are discussed in Sec. IV, and final conclusions and outlooks are given in Sec. V.

II. EXPERIMENTAL SETUP AND DATA REDUCTION

The experiment was carried out at Istituto Nazionale di Fisica Nucleare–Laboratori Nazionali del Sud (INFN-LNS) in Catania. The $^{18}O^{8+}$ ion beam was accelerated by the Superconducting Cyclotron at the energy of 275 MeV and impinged on a 270 $\mu g/cm^2$ ^{76}Se target, evaporated on a natural carbon foil 80 $\mu g/cm^2$ thick. Measurements using a natural carbon target (thickness 400 $\mu g/cm^2$) were performed to estimate and subtract the background contribution from the interaction of the beam with the target backing. The targets were produced at the LNS chemical laboratory. The thickness values were obtained by energy-loss measurements using an α-radioactive source with uncertainties of about $\pm 5\%$. A Faraday cup was used to stop the beam and measure the integrated electric charge.

The ^{19}F reaction ejectiles were analyzed in momentum by the MAGNEX large acceptance magnetic spectrometer [40]. The optical axis was centered at $\theta_{opt} = 8^\circ$ corresponding to an horizontal acceptance between 3° and 14° in the laboratory reference frame. The vertical acceptance was set to $\pm 1.75^\circ$. The parameters of the ion trajectories (i.e., vertical and horizontal positions and incident angles at the focal plane) were measured by the focal plane detector [51]. Thanks to the high angular, mass, and energy resolution of the apparatus and to the adopted particle identification technique [52–55], the $^{19}F^{9+}$ ions were unambiguously selected. Trajectory reconstruction of the ejectiles was performed solving the equation of motion for each detected particle [56] to extract scattering parameters at the target point. Further details of the data reduction technique can be found in Refs. [44,57–59]. The excitation energy E_x was calculated as the difference $Q_0 - Q$. Q_0 is the ground to ground state reaction Q-value and Q is the Q-value obtained by the missing mass calculations based on relativistic kinematic transformations.

The excitation energy spectrum of the ^{76}Se(^{18}O, ^{19}F)^{75}As reaction in the angular range between 4° and 4.5° is shown in Fig. 2. The background contribution, originating from the reaction ^{12}C(^{18}O, ^{19}F)^{11}B in the ^{76}Se target backing, is indicated by the dotted red line. The contribution due to the carbon contaminant is not negligible at excitation energies higher than 10 MeV. Therefore, it was subtracted after a proper normalization, which accounts for the peak at 10 MeV as a reference.

The energy differential cross section spectrum for the one-proton pickup reaction, after the carbon background subtraction, is shown in Figs. 3(a) and 3(b). The cross section is extracted taking into account the overall MAGNEX efficiency [58] following the technique described in Ref. [44]. The statistical uncertainty is included in the spectrum error bars in Fig. 3(b). A systematic error of about 10%, due to the determination of the beam collected charge and the target thickness, is common to all data points and it is not displayed in the figures. The achieved resolutions are δE(FWHM) $\approx$ 350 keV in energy and $\delta\theta_{lab}$(FWHM) $\approx 0.5^\circ$ in angle, similar to the

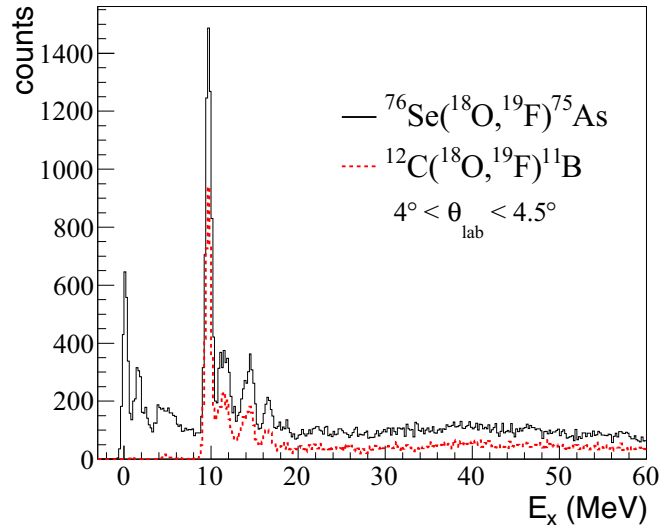

FIG. 2. Excitation energy spectrum for the ^{76}Se(^{18}O, ^{19}F)^{75}As (solid black line) and ^{12}C(^{18}O, ^{19}F)^{11}B (dotted red line) reactions at 275 MeV incident energy, in the angular range $4^\circ < \theta_{lab} < 4.5^\circ$.

one-neutron stripping reaction studied in Ref. [37]. Despite the good energy resolution, the structures observed in the spectrum do not coincide with isolated transitions because of the high level density of the residual nucleus.

Transfer reaction cross sections between heavy ions at energies well above the Coulomb barrier are maximized around optimal values of the Q-value (Q_{opt}) and transferred angular momentum (L_{opt}), as described in Ref. [60]. For the examined reaction the Q_{opt} value is -2.2 MeV while L_{opt} is 2. As a consequence of the negative Q_{opt}, the cross section decreases at increasing excitation energies, resulting in a larger cross section for transitions to the first low-lying states, as typical in these experimental conditions [37,38].

In Fig. 3(b) the energy differential cross section for the ^{76}Se(^{18}O, ^{19}F)^{75}As one-proton reaction at low excitation energy is shown. Two main peaks are visible, centered around 0.0 and 1.9 MeV. In this work two regions of interest (ROIs) are considered in the energy ranges $-0.6 < E_x < 0.8$ and $0.8 < E_x < 2.2$ MeV. The regions of the spectrum at higher excitation energies need further investigations to clarify which are the relevant states populated in the ejectile and residual nucleus.

The cross section angular distributions for the two energy regions of interest are plotted in Fig. 4. The uncertainties originating from the solid angle, the efficiency correction, and the statistical error are included in the error bars. The extracted angular distributions show the typical exponential decrease for angles larger than the grazing one ($\theta^{gr}_{c.m.} \approx 9^\circ$).[1]

[1] $\theta^{gr}_{c.m.} = 2\arcsin\left(\frac{V_C/\mu}{2E_{lab}/A_p - V_C/\mu}\right)$, where μ is the reduced mass of the colliding system; E_{lab} is the projectile incident energy in the laboratory reference frame; $V_C = \frac{Z_p Z_t e^2}{R_C}$; $R_C = 1.44(A_t^{1/3} + A_p^{1/3})$; and Z_p (A_p), Z_t (A_t) denote the charge (mass) number of projectile and target, respectively [61].

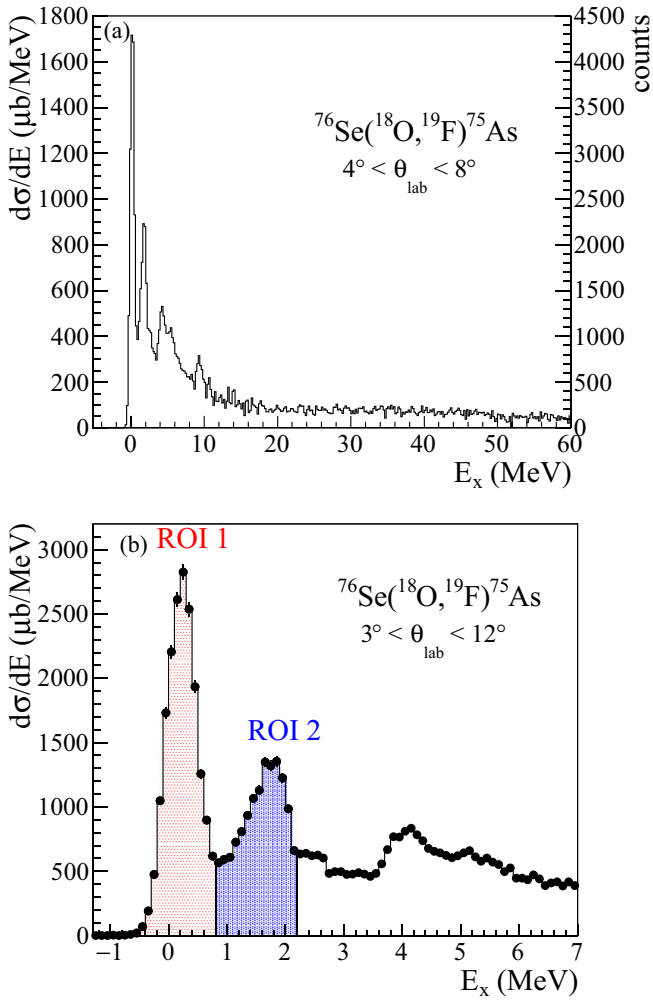

FIG. 3. (a) Differential cross section spectrum obtained for the ^{76}Se(^{18}O, ^{19}F) ^{75}As one-proton pickup reaction at 275 MeV in the angular range $4^\circ < \theta_{\rm lab} < 8^\circ$. (b) Zoomed view at low excitation energy for $3^\circ < \theta_{\rm lab} < 12^\circ$. The two regions of interest (ROIs) examined for the extraction of angular distributions are defined by the red and blue areas, respectively. The background contribution due to the presence of the ^{12}C backing in the target is subtracted.

III. THEORETICAL ANALYSIS

Nuclear structure calculations based on large-scale shell-model and interacting boson-fermion model are performed to derive the spectroscopic amplitudes for the projectile and target overlaps. For the reaction modeling distorted wave Born approximation (DWBA), coupled-channels Born approximation (CCBA), and coupled reaction channel (CRC) approaches are adopted to single out the effect of specific channel couplings in the measured cross section.

A. Shell-model calculations

The spectroscopic amplitudes for both projectile and target overlaps were computed within the shell-model framework, using the KSHELL [62] code.

Regarding the $\langle ^{19}\mathrm{F} \,|\, ^{18}\mathrm{O}\rangle$ projectile overlaps, shell-model calculations adopting the *psdmod* [63] interaction were performed. This interaction is a modified version of the PSDWBT one [64], that assumes ^{4}He as a closed core and $0p_{1/2}$, $0p_{3/2}$, $0d_{3/2}$, $0d_{5/2}$, and $1s_{1/2}$ as valence orbits included in the model space for both protons and neutrons. It has been successfully used in our previous studies (e.g., [30,34,37]) and, recently, for computing also the one-proton pickup spectroscopic amplitudes related to $\langle ^{19}\mathrm{F} \,|\, ^{18}\mathrm{O}\rangle$ [10,36,38].

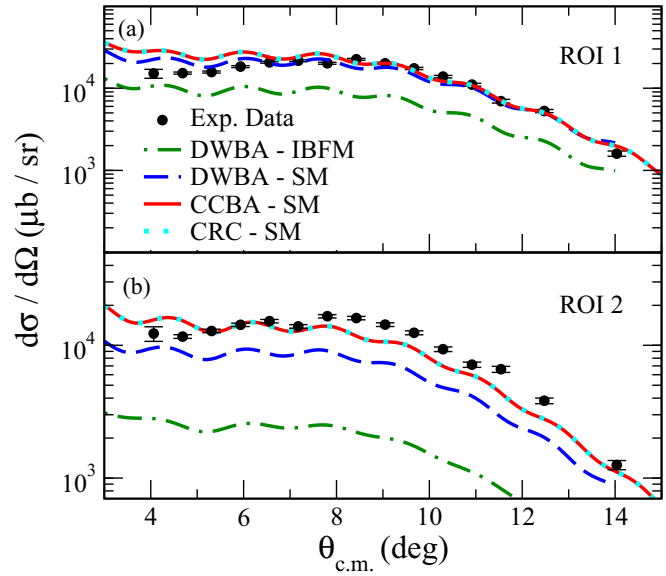

FIG. 4. Comparison between the theoretical curves and experimental points for one-proton transfer angular distribution. The angular distributions related to the contribution of the unresolved excited states of the first and second ROIs in Fig. 3(b) are shown. The DWBA (dashed blue line), CCBA (continuous red line), and CRC (dotted cyan line) calculations obtained using shell-model spectroscopic amplitudes (SM) are shown together with DWBA (dotted-dashed green line) calculations obtained using spectroscopic amplitudes from the interacting boson-fermion model (IBFM) for the target and from the shell model for the projectile (see text).

In Table I, we report the calculated spectroscopic factors together with the values extracted from $(^3\mathrm{He}, d)$ [65,66], (α, t) [67], and (p, γ) [68] reactions and the corresponding experimental level energies. The spectroscopic factors from different experiments are characterized by significant differences, going beyond the estimated uncertainties (20–25%), which may be due to inaccuracies in the modeling of the reaction dynamics as well as to computational limits, espe-

TABLE I. ^{19}F energy levels and related spectroscopic factors S from Refs. [65–68] and from shell-model (SM) calculations. Energies are in MeV.

$E_x(^{19}\mathrm{F})$	n, l, j	S [65]	S [66]	S [67]	S [68]	S (SM)
0.000	$2s_{1/2}$	0.21	0.30	0.25	0.18	0.31
0.110	$1p_{1/2}$	0.11	0.12			0.06
0.197	$1d_{5/2}$	0.41	0.42	0.67	0.37	0.44
1.458	$1p_{3/2}$	0.024	0.036			0.0001
1.554	$1d_{3/2}$	0.25	0.29	0.41	0.25	0.18

TABLE II. Proton and neutron single particle energies adopted in the calculation.

π (nlj)	ϵ_π (MeV)	ϵ_ν (MeV)
$0f_{5/2}$	1.0	0.8
$1p_{3/2}$	0.0	0.0
$1p_{1/2}$	1.1	1.1
$0g_{9/2}$	3.2	3.2

cially when old studies are considered [69]. This situation prevents a sound test of our results. However, the numbers of Table I also evidence that our shell-model calculations provide a reasonable description of the single-particle nature of the ^{19}F states.

For the $\langle {}^{76}\mathrm{Se} \,|\, {}^{75}\mathrm{As}\rangle$ overlaps, the interaction successfully used in Ref. [37] was adopted. In such an interaction ^{56}Ni is considered as a closed inert core with protons and neutrons in the valence space made up of $0f_{5/2}$, $1p_{3/2}$, $1p_{1/2}$, and $0g_{9/2}$ orbitals. The effective Hamiltonian, already employed to study the structure of ^{66}Zn and the β-decay properties of ^{76}Ge, ^{82}Se [70,71], was derived within the framework of many-body perturbation theory from the CD-Bonn nucleon-nucleon potential [72] renormalized by way of the $V_{\text{low-k}}$ approach [73] with the addition of the Coulomb potential for protons. In particular, the two-body matrix elements have been calculated within the $\hat{Q}$-box folded-diagram approach [74], including in the perturbative expansion of the $\hat{Q}$-box one- and two-body diagrams up to the third order in the interaction.

The single-neutron and single-proton energies are listed in Table II, and they were taken from the experimental energy spectra of ^{57}Ni [75] and ^{57}Cu [75], respectively, except for the $0g_9/2$ orbital. As a matter of fact, no level with $J^\pi = 9/2^+$ has been identified in ^{57}Cu, while for ^{57}Ni the state observed in the fusion-evaporation reaction $^{28}\mathrm{Si}(^{32}\mathrm{S}, 2pn)\,^{57}\mathrm{Ni}$ at 3.7 MeV has been interpreted as the neutron $0g_{9/2}$ single-particle state [76]. In addition, at about 3 MeV a state with a disputed $7/2+$ or $9/2+$ spin-parity is known.

One possible strategy is to choose the proton $0g_{9/2}$ orbital at the same energy of the neutron one, as was down in Refs. [37,71]. Here, an estimated effective single-particle energy of 3.2 MeV is used for both neutron and proton $0g_{9/2}$ orbitals. From the proton side, this value results from an analysis of the $N = 50$ isotones from $Z = 40$ to 48 [77]. As concerns the neutron $0g_{9/2}$ orbital, we have verified that a lowering of its location leads to a slightly better agreement between the experimental and calculated spectra of ^{75}As, as also evidenced in previous shell-model calculations for Ge and Ga isotopes [78–80]. It is worth nothing that these variations in the single-particle energies of the $0g_{9/2}$ orbital do not significantly affect the calculated spectroscopic amplitudes.

The theoretical excitation energies of the ^{19}F, ^{18}O, ^{76}Se, and ^{75}As states considered in the cross section calculations are given in Table III. Comparing theoretical and experimental values, a reasonably good agreement is found for most of the ^{19}F, ^{18}O, and ^{76}Se states. The even-odd ^{75}As nucleus presents a more complex spectrum with more than 60 states in the considered regions of interest [75]. However, not all of them

TABLE III. Comparison between theoretical and experimental low-lying excitation energies for the ^{18}O, ^{19}F, ^{76}Se and ^{75}As nuclei obtained by large-scale shell-model (SM) and interacting boson-fermion model calculations (IBFM). Energies are in MeV.

Nucleus	J^π	$E_{\text{EXP.}}$	E_{SM}	E_{IBFM}
	0^+	0.000	0.000	
^{18}O	2^+	1.982	2.264	
	3^-	5.097	4.929	
	$1/2^+$	0.000	0.107	
	$1/2^-$	0.110	0.744	
^{19}F	$5/2^+$	0.197	0.000	
	$5/2^-$	1.345	2.422	
	$3/2^-$	1.458	2.615	
	$3/2^+$	1.554	1.080	
^{76}Se	0^+	0.000	0.000	
	2^+	0.559	0.753	
	$3/2^-$	0.000	0.072	0.000
	$1/2^-$	0.199	0.240	0.198
	$3/2^-$	0.265	0.808	0.490
	$5/2^-$	0.280	0.000	0.152
	$9/2^+$	0.304	1.100	0.286
	$1/2^-$	0.469	0.519	0.462
	$5/2^-$	0.572	0.655	0.554
	$1/2^-$	0.585	1.758	0.862
	$3/2^-$	0.618	1.085	0.679
	$7/2^-$	0.822	0.685	
^{75}As	$7/2^-$	1.043	1.210	
	$3/2^-$	1.074	1.311	0.866
	$3/2^-$	1.127	1.856	1.282
	$9/2^+$	1.261	2.546	1.249
	$7/2^-$	1.309	2.203	
	$5/2^-$	1.420	1.054	0.718
	$9/2^+$	1.430	2.581	1.515
	$1/2^-$	1.606	2.439	1.283
	$5/2^-$	1.660	1.519	0.894
	$7/2^-$	1.691	2.380	
	$9/2^+$	1.808	2.592	1.978
	$1/2^-$	1.878	2.576	1.486
	$7/2^-$	1.928	2.564	
	$1/2^-$	2.021	2.787	
	$5/2^-$	2.210	1.764	1.337

are expected to be strongly populated in one-proton pickup reactions as observed in $(d, {}^3\mathrm{He})$ reactions [81,82]. For that reason, in our analysis we focus on the states observed in Refs. [81,82]. In addition, a large model space is likely to be adopted to describe this mid-shell nucleus down to low-lying states. This could explain the slightly worse agreement that we observe for the spectrum of ^{75}As, as reported in Table III, where most of the excited states are significantly above the experimental energies. These discrepancies may highlight the need of a larger model space in the structure calculations, as discussed in Ref. [37]. On the other hand, it should be considered that the adopted Hamiltonian (see Ref. [71]) is developed for systems with two valence particles, while ^{75}As is a system with 19 valence nucleons. This means that one should derive an effective Hamiltonian which takes into account the filling of the model space orbitals, as done in Refs. [83,84]. However,

TABLE IV. Shell-model (SM) spectroscopic amplitudes (SA) for the projectile overlaps used in DWBA and CCBA (CRC) calculations. The symbols n, l, and j correspond to the principal quantum number and the orbital and the total angular momenta of the transferred proton orbitals, respectively.

Initial state	nlj	Final state	SA_{SM}
	$2s_{1/2}$	$^{19}F_{g.s.}(1/2^+)$	−0.5539
	$1p_{1/2}$	$^{19}F_{0.110}(1/2^-)$	−0.2444
$^{18}O_{g.s.}(0^+)$	$1d_{5/2}$	$^{19}F_{0.197}(5/2^+)$	0.6644
	$1p_{3/2}$	$^{19}F_{1.458}(3/2^-)$	−0.0106
	$1d_{3/2}$	$^{19}F_{1.554}(3/2^+)$	−0.4238
	$1d_{5/2}$	$^{19}F_{g.s.}(1/2^+)$	0.5864
	$1d_{3/2}$	$^{19}F_{g.s.}(1/2^+)$	−0.2806
	$1p_{3/2}$	$^{19}F_{0.110}(1/2^-)$	−0.0301
	$1d_{5/2}$	$^{19}F_{0.197}(5/2^+)$	−0.4265
	$2s_{1/2}$	$^{19}F_{0.197}(5/2^+)$	−0.3113
$^{18}O_{1.982}(2^+)$	$1d_{3/2}$	$^{19}F_{0.197}(5/2^+)$	0.1563
	$1p_{3/2}$	$^{19}F_{1.345}(5/2^-)$	0.0186
	$1p_{1/2}$	$^{19}F_{1.345}(5/2^-)$	0.1366
	$1p_{3/2}$	$^{19}F_{1.458}(3/2^-)$	−0.0022
	$1p_{1/2}$	$^{19}F_{1.458}(3/2^-)$	0.1639
	$1d_{5/2}$	$^{19}F_{1.554}(3/2^+)$	0.3146
	$2s_{1/2}$	$^{19}F_{1.554}(3/2^+)$	0.3539
	$1d_{3/2}$	$^{19}F_{1.554}(3/2^+)$	0.3185
	$1d_{5/2}$	$^{19}F_{0.110}(1/2^-)$	−0.4906
	$1p_{1/2}$	$^{19}F_{0.197}(5/2^+)$	0.5849
	$1p_{3/2}$	$^{19}F_{0.197}(5/2^+)$	−0.0900
	$1d_{3/2}$	$^{19}F_{1.345}(5/2^-)$	-0.0268
$^{18}O_{5.097}(3^-)$	$1d_{5/2}$	$^{19}F_{1.345}(5/2^-)$	−0.4864
	$2s_{1/2}$	$^{19}F_{1.345}(5/2^-)$	−0.3768
	$1d_{3/2}$	$^{19}F_{1.458}(3/2^-)$	0.0486
	$1d_{5/2}$	$^{19}F_{1.458}(3/2^-)$	0.2614
	$1p_{3/2}$	$^{19}F_{1.554}(3/2^+)$	0.1675

based on our previous calculations [70,71], we can assert that the limitations of the present calculations affect more significantly the energy spectra than the wave functions, as recently proved adopting the same Hamiltonian to derive the spectroscopic amplitudes for the similar one-neutron stripping case [85]. The calculated spectroscopic amplitudes are listed in Tables IV and V for the projectile and target overlaps, respectively.

The calculated spectroscopic factors for ^{75}As can be compared to the experimental values of Refs. [81,82]. The corresponding table is not reported here to avoid a further overloading of the paper. We only mention that, although the two sets of experimental data show notable differences, even larger than those shown for the ^{19}F case, the comparison between theory and experiment reveals certain deficiencies in the single-particle strength description of some states. This may be related to the adopted model space, which for ^{76}Se and ^{75}As is restricted to one major proton and neutron shell, or to inaccuracies in the matrix elements of our two-body interaction, which as, mentioned above, is microscopically derived without employing any adjustable parameters.

TABLE V. Shell-model (SM) and interacting boson-fermion model (IBFM) spectroscopic amplitudes (SA) for the target overlaps used in DWBA and CCBA (CRC) calculations. The symbols n, l, and j correspond to the principal quantum number and the orbital and the total angular momenta of the transferred proton orbitals, respectively.

Initial state	nlj	Final state	SA_{SM}	SA_{IBFM}
	$1p_{3/2}$	$^{75}As_{g.s.}(3/2^-)$	1.3584	−0.6220
	$1p_{1/2}$	$^{75}As_{0.199}(1/2^-)$	0.3990	0.8630
	$1p_{3/2}$	$^{75}As_{0.265}(3/2^-)$	−0.2800	0.0520
	$0f_{5/2}$	$^{75}As_{0.280}(5/2^-)$	−1.2155	0.8580
	$0g_{9/2}$	$^{75}As_{0.304}(9/2^+)$	−0.5041	0.9560
	$1p_{1/2}$	$^{75}As_{0.469}(1/2^-)$	0.7797	0.0970
	$0f_{5/2}$	$^{75}As_{0.572}(5/2^-)$	−0.3123	−0.0180
	$1p_{1/2}$	$^{75}As_{0.585}(1/2^-)$	0.0391	0.0000
	$1p_{1/2}$	$^{75}As_{0.618}(3/2^-)$	0.4534	0.0390
$^{76}Se_{g.s.}(0^+)$	$1p_{3/2}$	$^{75}As_{1.074}(3/2^-)$	0.6509	−0.0820
	$1p_{3/2}$	$^{75}As_{1.127}(3/2^-)$	−0.0737	0.0570
	$0g_{9/2}$	$^{75}As_{1.261}(9/2^+)$	0.0490	0.1480
	$0f_{5/2}$	$^{75}As_{1.420}(5/2^-)$	0.1813	0.0130
	$0g_{9/2}$	$^{75}As_{1.430}(9/2^+)$	0.1124	−0.0350
	$1p_{1/2}$	$^{75}As_{1.606}(1/2^-)$	0.1352	0.0000
	$0f_{5/2}$	$^{75}As_{1.660}(5/2^-)$	−0.2691	0.0000
	$0g_{9/2}$	$^{75}As_{1.808}(9/2^+)$	0.0285	−0.0140
	$1p_{1/2}$	$^{75}As_{1.878}(1/2^-)$	−0.0254	0.0220
	$0f_{5/2}$	$^{75}As_{2.210}(5/2^-)$	0.1704	−0.0130
	$0f_{5/2}$	$^{75}As_{g.s.}(3/2^-)$	−0.0688	
	$1p_{3/2}$	$^{75}As_{g.s.}(3/2^-)$	0.1716	
	$1p_{1/2}$	$^{75}As_{g.s.}(3/2^-)$	−0.3922	
	$0f_{5/2}$	$^{75}As_{0.199}(1/2^-)$	−0.1954	
	$1p_{3/2}$	$^{75}As_{0.199}(1/2^-)$	−0.0883	
	$of_{5/2}$	$^{75}As_{0.265}(3/2^-)$	−0.1175	
	$1p_{3/2}$	$^{75}As_{0.265}(3/2^-)$	−0.0888	
	$1p_{1/2}$	$^{75}As_{0.265}(3/2^-)$	0.4171	
	$0f_{5/2}$	$^{75}As_{0.280}(5/2^-)$	0.8113	
	$1p_{3/2}$	$^{75}As_{0.280}(5/2^-)$	0.0822	
	$1p_{1/2}$	$^{75}As_{0.280}(5/2^-)$	0.0893	
	$0g_{9/2}$	$^{75}As_{0.304}(9/2^+)$	0.3290	
$^{76}Se_{0.559}(2^+)$	$0g_{9/2}$	$^{75}As_{0.401}(5/2^+)$	−0.0219	
	$0f_{5/2}$	$^{75}As_{0.469}(1/2^-)$	−0.1014	
	$1p_{3/2}$	$^{75}As_{0.469}(1/2^-)$	0.4312	
	$0f_{5/2}$	$^{75}As_{0.572}(5/2^-)$	0.0153	
	$1p_{3/2}$	$^{75}As_{0.572}(5/2^-)$	−0.6646	
	$1p_{1/2}$	$^{75}As_{0.572}(5/2^-)$	−0.2198	
	$0f_{5/2}$	$^{75}As_{0.585}(1/2^-)$	−0.0743	
	$1p_{1/2}$	$^{75}As_{0.585}(1/2^-)$	−0.0088	
	$of_{5/2}$	$^{75}As_{0.618}(3/2^-)$	0.0415	
	$1p_{3/2}$	$^{75}As_{0.618}(3/2^-)$	−0.3617	
	$1p_{1/2}$	$^{75}As_{0.618}(3/2^-)$	0.1626	
	$0f_{5/2}$	$^{75}As_{0.822}(7/2^-)$	−0.7509	
	$1p_{3/2}$	$^{75}As_{0.822}(7/2^-)$	0.2539	
	$0f_{5/2}$	$^{75}As_{1.043}(7/2^-)$	−0.2312	
	$1p_{3/2}$	$^{75}As_{1.043}(7/2^-)$	−0.6971	
	$0f_{5/2}$	$^{75}As_{1.074}(3/2^-)$	−0.1674	
	$1p_{3/2}$	$^{75}As_{1.074}(3/2^-)$	−0.5776	
	$1p_{1/2}$	$^{75}As_{1.074}(3/2^-)$	0.1047	
	$0f_{5/2}$	$^{75}As_{1.127}(3/2^-)$	0.0161	
	$1p_{3/2}$	$^{75}As_{1.127}(3/2^-)$	0.0666	
	$1p_{1/2}$	$^{75}As_{1.127}(3/2^-)$	0.0656	
$^{76}Se_{0.559}(2^+)$	$0g_{9/2}$	$^{75}As_{1.261}(9/2^+)$	0.0490	

TABLE V. *(Continued).*

Initial state	nlj	Final state	SA_{SM}	SA_{IBFM}
	$0f_{5/2}$	$^{75}As_{1.309}(7/2^-)$	−0.1795	
	$1p_{3/2}$	$^{75}As_{1.309}(7/2^-)$	0.2347	
	$0f_{5/2}$	$^{75}As_{1.420}(5/2^-)$	0.2371	
	$1p_{3/2}$	$^{75}As_{1.420}(5/2^-)$	−0.4218	
	$1p_{1/2}$	$^{75}As_{1.420}(5/2^-)$	−0.5010	
	$0g_{9/2}$	$^{75}As_{1.430}(9/2^+)$	0.0465	
	$0f_{5/2}$	$^{75}As_{1.606}(1/2^-)$	−0.0764	
	$1p_{3/2}$	$^{75}As_{1.606}(1/2^-)$	0.0597	
	$0f_{5/2}$	$^{75}As_{1.660}(5/2^-)$	0.0954	
	$1p_{1/2}$	$^{75}As_{1.660}(5/2^-)$	−0.0324	
	$1p_{1/2}$	$^{75}As_{1.660}(5/2^-)$	0.2223	
	$0f_{5/2}$	$^{75}As_{1.691}(7/2^-)$	−0.0350	
	$1p_{3/2}$	$^{75}As_{1.691}(7/2^-)$	0.1077	
	$0g_{9/2}$	$^{75}As_{1.808}(9/2^+)$	0.0199	
	$0f_{5/2}$	$^{75}As_{1.878}(1/2^-)$	−0.0122	
	$1p_{1/2}$	$^{75}As_{1.878}(1/2^-)$	−0.0287	
	$0f_{5/2}$	$^{75}As_{1.928}(7/2^-)$	−0.1316	
	$1p_{3/2}$	$^{75}As_{1.928}(7/2^-)$	0.3070	
	$0f_{5/2}$	$^{75}As_{2.210}(5/2^-)$	0.0308	
	$1p_{3/2}$	$^{75}As_{2.210}(5/2^-)$	0.5030	
	$1p_{1/2}$	$^{75}As_{2.210}(5/2^-)$	−0.3113	

B. Interacting boson-fermion model

Spectroscopic amplitudes for $\langle ^{76}Se\,|\,^{75}As\rangle$ overlaps were calculated also within the formalism of the interacting boson-fermion model (IBFM-2).

In the interacting moson model 2 (IBM-2), the collective properties of a even-even nucleus are described using a system of bosons with angular momentum 0 or 2 [86]. The IBM-2 can be extended for the analysis of odd-even nuclei in the IBFM-2 by introducing an additional single-particle degree of freedom coupled to the boson system [87]. The IBM-2 and IBFM-2 were previously used in similar calculations in Refs. [34,35], including the case of ^{76}Se(^{18}O, ^{17}O) ^{77}Se reaction at the same energy in Ref. [37].

The odd-fermion Hamiltonian [87,88] and the quasiparticle energy of the odd particle are calculated in the Bardeen-Cooper-Schrieffer (BCS) approximation [89–93].

^{75}As has 33 protons and 42 neutrons, which implies ^{75}As has 5 valence protons in the shell 28-50. In the IBFM, these 5 valence protons are seen as 2 proton bosons plus an uncoupled proton. To find the even-even nucleus that corresponds to ^{75}As, we consider the even-even nucleus that has 2 proton bosons in the shell 28-50. This leads us to ^{74}Ge. Therefore, the construction of ^{75}As involves coupling one proton to the core ^{74}Ge. We use the same four orbitals $0f_{5/2}$, $1p_{3/2}$, $1p_{1/2}$, and $0g_{9/2}$ that we used in the shell-model calculations. The proton quasiparticle energies and occupation probabilities, calculated by solving the BCS equations, are displayed in Table VI. The proton single-particle energies of ^{75}As, E_{j_π}, required by the BCS calculation are taken from Ref. [94]. The E_{j_π} are consistent with the ones employed in the shell-model calculations (Table II).

TABLE VI. Proton single-particle energies E_{j_π}, quasiparticle energies Q_{spe}, and occupation probabilities v^2 of ^{75}As used in the present IBFM-2 model calculations.

Orbit j_π	E_{j_π} (MeV)	Q_{spe} (MeV)	v^2
$0f_{5/2}$	1.0280	1.5747	0.2624
$0g_{9/2}$	3.0090	3.0608	0.0542
$1p_{3/2}$	0.0000	1.4136	0.5990
$1p_{1/2}$	1.1060	1.6133	0.2439

A comparison between the calculated and experimental energy spectra for the ^{75}As nucleus is given in Table III while the spectroscopic amplitudes are listed in Table V.

C. Reaction calculations

Cross section calculations adopting the distorted wave Born approximation (DWBA), the coupled-channels Born approximation (CCBA), and the coupled reaction channel (CRC) approaches using the FRESCO code [95,96] were performed for the ^{76}Se(^{18}O, ^{19}F) ^{75}As reaction. The states included in the coupling scheme are sketched in Fig. 5.

The optical potential for the initial partition was chosen according to the elastic and inelastic scattering and one-neutron stripping [37] analysis of the ^{18}O + ^{76}Se collision at the same energy described in Ref. [46], as required by the multichannel approach [10–12]. For the description of both the real and imaginary parts of the optical potential, the double-folding São Paulo potential [97] was adopted to generate the distorted waves at the entrance and exit channels. The same geometry is used for both the real and imaginary parts, with a scaling factor N_i properly determined for the imaginary part of the potential. For DWBA calculations the standard choice [98–100] is $N_i = 0.78$ for both initial and final partition. For CCBA and CRC calculations, $N_i = 0.78$ for the final partition and $N_i = 0.6$ is chosen in the initial partition to account for all the channels not explicitly included in the system of coupled equations, like fusion and coupling to higher excitation energy bound and continuum states [101]. Such prescriptions for the optical potentials have been successfully used in many studies of scattering, transfer, and charge exchange reactions [11,12,14,26–31,34–40,45,46,102–107]. In addition, a study of the sensitivity of the results to the N_i value of the imaginary part was performed in Ref. [37]. It was highlighted that when varying N_i within 20% from the standard values the transfer cross sections are not significantly affected. However, if $N_i = 0.6$ is chosen in the initial partition, a superior agreement between theory and experiment is achieved. The transfer operator was calculated in the post representation including full complex remnant terms, as done in Ref. [38].

The single-particle wave functions are generated adopting, as core effective interactions, Woods-Saxon potentials. The reduced radius r_0 and the diffuseness a_0 are equal to 1.26 fm and 0.70 fm [11,30,102], respectively. For the heavier target-like system $r_0 = 1.20$ fm and $a_0 = 0.60$ fm were adopted, as typically done when considering similar medium-mass nuclei [31,34,36–38]. The depths of such Woods-Saxon potentials

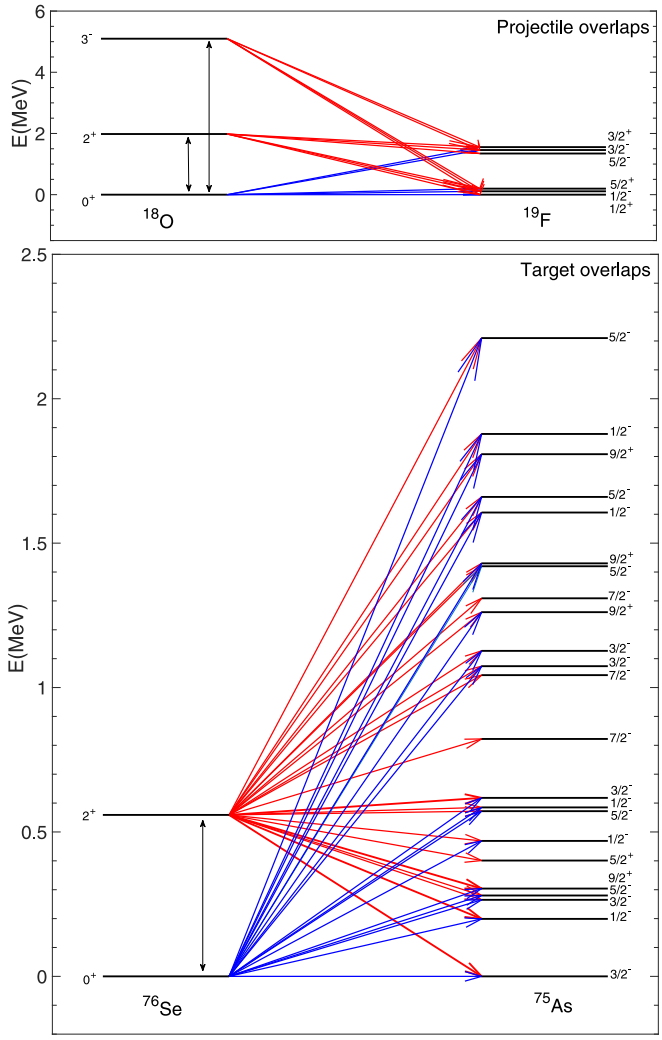

FIG. 5. Coupling schemes for the projectile and target overlaps considered in one-proton transfer calculations. The blue arrows correspond to the only couplings included in DWBA calculations. CCBA also includes the couplings represented by red and black arrows. CRC includes the same couplings as CCBA but at infinite order.

were adjusted in order to reproduce the experimental one-proton separation energies.

In previous elastic and inelastic scattering analyses [10,46] the inclusion of the first 2^+ of the projectile and target and the first 3^- of the ^{18}O collective low-lying excited states turned out to be important to well describe the angular distributions over the full range of transferred momenta explored. Therefore, in the CCBA and CRC calculations, inelastic excitations to the low-lying states of the projectile and target nuclei were taken into account by adopting the rotational model. Coulomb deformations for ^{18}O and ^{76}Se are introduced in terms of the reduced transition probabilities $B(E_\lambda)$, where λ is the multipolarity of the excitation, as described in Ref. [46]. $B(E2; 0^+ \to 2^+) = 0.0043\ e^2\mathrm{b}^2$ and $B(E3; 0^+ \to 3^-) = 0.00046\ e^2\mathrm{b}^3$ are used in the coupling scheme to consider the excitation to the first 2^+ and 3^- ^{18}O states, respectively. For ^{76}Se target $B(E2; 0^+ \to 2^+) = 0.4320\ e^2\mathrm{b}^2$ is considered. The $B(E_\lambda)$ adopted are taken from experimental data (see Refs. [108,109]), but they are similar to those obtained from shell-model calculations [37]. The effective charges adopted for determining the $B(E_\lambda)$ have been calculated consistently with the Hamiltonian by employing the Suzuki-Okamoto formalism [110]. The signs of the reduced matrix elements $M(E_\lambda)$ are obtained from shell-model calculations, according to the phase convention of the wave functions used to determine the spectroscopic amplitudes. All details about the procedure can be found in [70].

In the one-neutron stripping analysis of the same system ($^{18}\mathrm{O} + {}^{76}\mathrm{Se}$), we found that the effect on the calculated cross sections of the final partition couplings is much smaller than the initial one. Therefore, couplings between the ^{75}As states are not considered in the present analysis.

IV. DISCUSSION

In Fig. 4 the comparison between the theoretical and experimental angular distributions for the energy regions corresponding to the two mentioned ROIs of Fig. 3(b) is shown. A remarkable agreement between theoretical and experimental cross sections is obtained considering that no arbitrary scaling factors are used in the calculations. In addition, the diffraction pattern of the DWBA and CCBA or CRC curves is similar to the experimental data.

Comparing DWBA and CCBA (CRC) calculations, CCBA results give a larger cross section and a slightly different diffraction pattern compared to DWBA. The inclusion of inelastic excitations of projectile and target in the coupling scheme, respectively through $^{18}\mathrm{O}^{2+}{}_1$, $^{18}\mathrm{O}^{3-}_1$ and $^{76}\mathrm{Se}^{2+}{}_1$ states, improves the agreement with the experimental data. This is particularly true in the case of ROI 2. Actually, considering the integrated cross section, listed in Table VII, we evince an enhancement in CCBA calculations with respect to DWBA of about 15% in ROI 1 and 50% in ROI 2. Moreover, as observed for other one-nucleon transfer reactions in similar experimental conditions [10,11,37], the inclusion of couplings among different partition to infinite order (CRC) does not change the obtained results. As is evident in Fig. 4, the curves related to CRC calculations are practically superimposed on the CCBA ones. This outcome highlights the minor importance of the back-coupling of the transfer on the elastic channel, when focusing in the angular window we are considering corresponding to a significant momentum transfer ($0.9 < q < 3$ fm^{-1}).

To gain more insight, we have analyzed in detail the angular distributions shown in panels (a) and (b) of Fig. 4 for ROI 1 and ROI 2, respectively. In Figs. 6 the most relevant transitions for each ROI are shown together with the sum of all the contributing transitions for DWBA and CCBA calculations and the experimental data. The sum of the other, less relevant transitions is also shown. The nuclear transitions which contribute more to ROI 1 (see Table VII) are those feeding the $^{19}\mathrm{F}_{0.197\ \mathrm{MeV}}(5/2^+)$ state in connection with the ground state, the first $5/2^-$ state at $E_x = 0.280$ MeV, and the second $1/2^-$ state at $E_x = 0.469$ MeV of ^{75}As. The transition to the $^{19}\mathrm{F}_{\mathrm{g.s.}}$ in connection with $^{75}\mathrm{As}_{\mathrm{g.s.}}$ is contributing as well. Although a better agreement is obtained when considering CCBA, the

TABLE VII. One-proton transfer theoretical cross sections (in μb) integrated in the angular range [0°, 20°] of the laboratory system and for all the combination of projectile and target states lying within the two ROIs in Fig. 3.

Final channel	DWBA SM	CCBA SM	DWBA IBFM
ROI 1			
$^{19}F_{g.s.}(1/2^+) + {}^{75}As_{g.s.}(3/2^-)$	296.83	308.82	62.24
$^{19}F_{0.110}(1/2^-) + {}^{75}As_{g.s.}(3/2^-)$	32.00	33.59	6.71
$^{19}F_{0.197}(5/2^+) + {}^{75}As_{g.s.}(3/2^-)$	1278.10	1293.30	267.97
$^{19}F_{g.s.}(1/2^+) + {}^{75}As_{0.199}(1/2^-)$	24.85	43.06	116.25
$^{19}F_{g.s.}(1/2^+) + {}^{75}As_{0.265}(3/2^-)$	12.11	9.54	0.42
$^{19}F_{g.s.}(1/2^+) + {}^{75}As_{0.280}(5/2^-)$	60.27	137.37	30.03
$^{19}F_{g.s.}(1/2^+) + {}^{75}As_{0.304}(9/2^+)$	5.81	15.36	20.91
$^{19}F_{0.110}(1/2^-) + {}^{75}As_{0.199}(1/2^-)$	3.83	6.54	17.90
$^{19}F_{0.110}(1/2^-) + {}^{75}As_{0.265}(3/2^-)$	1.33	1.07	0.05
$^{19}F_{0.110}(1/2^-) + {}^{75}As_{0.280}(5/2^-)$	9.40	22.54	4.69
$^{19}F_{0.197}(5/2^+) + {}^{75}As_{0.199}(1/2^-)$	88.13	124.23	412.29
$^{19}F_{0.110}(1/2^-) + {}^{75}As_{0.304}(9/2^+)$	0.81	1.74	2.93
$^{19}F_{0.197}(5/2^+) + {}^{75}As_{0.265}(3/2^-)$	53.63	48.37	1.85
$^{19}F_{g.s.}(1/2^+) + {}^{75}As_{0.469}(1/2^-)$	91.00	91.33	1.41
$^{19}F_{0.197}(5/2^+) + {}^{75}As_{0.280}(5/2^-)$	276.47	449.90	137.76
$^{19}F_{0.197}(5/2^+) + {}^{75}As_{0.304}(9/2^+)$	62.63	55.00	117.34
$^{19}F_{g.s.}(1/2^+) + {}^{75}As_{0.572}(5/2^-)$	3.70	4.63	0.01
$^{19}F_{0.110}(1/2^-) + {}^{75}As_{0.469}(1/2^-)$	14.10	15.37	0.22
$^{19}F_{g.s.}(1/2^+) + {}^{75}As_{0.618}(3/2^-)$	2.67	58.32	0.22
$^{19}F_{0.197}(5/2^+) + {}^{75}As_{0.469}(1/2^-)$	336.14	333.73	5.20
$^{19}F_{0.110}(1/2^-) + {}^{75}As_{0.572}(5/2^-)$	0.58	0.68	<0.01
$^{19}F_{0.110}(1/2^-) + {}^{75}As_{0.618}(3/2^-)$	0.42	6.02	0.03
$^{19}F_{0.197}(5/2^+) + {}^{75}As_{0.572}(5/2^-)$	17.75	15.27	0.06
ROI 2			
$^{19}F_{0.197}(5/2^+) + {}^{75}As_{0.618}(3/2^-)$	10.10	211.47	1.02
$^{19}F_{g.s.}(1/2^+) + {}^{75}As_{0.822}(7/2^-)$		5.75	
$^{19}F_{0.110}(1/2^-) + {}^{75}As_{0.822}(7/2^-)$		0.68	
$^{19}F_{0.197}(5/2^+) + {}^{75}As_{0.822}(7/2^-)$		15.02	
$^{19}F_{g.s.}(1/2^+) + {}^{75}As_{1.074}(3/2^-)$	57.56	105.66	0.91
$^{19}F_{0.110}(1/2^-) + {}^{75}As_{1.074}(3/2^-)$	6.78	109.75	0.11
$^{19}F_{0.197}(5/2^+) + {}^{75}As_{1.074}(3/2^-)$	277.32	409.47	4.40
$^{19}F_{g.s.}(1/2^+) + {}^{75}As_{1.309}(7/2^-)$		1.65	
$^{19}F_{1.346}(5/2^-) + {}^{75}As_{g.s.}(3/2^-)$		0.25	
$^{19}F_{0.110}(1/2^-) + {}^{75}As_{1.309}(7/2^-)$		0.16	
$^{19}F_{g.s.}(1/2^+) + {}^{75}As_{1.420}(5/2^-)$		11.36	
$^{19}F_{1.459}(3/2^-) + {}^{75}As_{g.s.}(3/2^-)$	0.14	0.18	0.03
$^{19}F_{0.197}(5/2^+) + {}^{75}As_{1.309}(7/2^-)$		0.16	
$^{19}F_{0.110}(1/2^-) + {}^{75}As_{1.420}(5/2^-)$		1.74	
$^{19}F_{1.346}(5/2^-) + {}^{75}As_{0.199}(1/2^-)$		0.04	
$^{19}F_{1.554}(3/2^+) + {}^{75}As_{g.s.}(3/2^-)$	321.06	345.34	67.31
$^{19}F_{1.346}(5/2^-) + {}^{75}As_{0.265}(3/2^-)$		0.01	
$^{19}F_{0.197}(5/2^+) + {}^{75}As_{1.420}(5/2^-)$	5.52	32.60	0.03
$^{19}F_{1.346}(5/2^-) + {}^{75}As_{0.280}(5/2^-)$		0.33	
$^{19}F_{1.346}(5/2^-) + {}^{75}As_{0.304}(9/2^+)$		0.04	
$^{19}F_{1.459}(3/2^-) + {}^{75}As_{0.199}(1/2^-)$	0.01	0.03	0.05
$^{19}F_{1.459}(3/2^-) + {}^{75}As_{0.265}(3/2^-)$	<0.01	<0.01	<0.01
$^{19}F_{1.459}(3/2^-) + {}^{75}As_{0.280}(5/2^-)$	0.02	0.11	0.01
$^{19}F_{1.459}(3/2^-) + {}^{75}As_{0.304}(9/2^+)$	<0.01	0.01	<0.01
$^{19}F_{1.554}(3/2^+) + {}^{75}As_{0.199}(1/2^-)$	34.63	58.40	162.02
$^{19}F_{1.346}(5/2^-) + {}^{75}As_{0.469}(1/2^-)$		0.07	
$^{19}F_{1.554}(3/2^+) + {}^{75}As_{0.265}(3/2^-)$	13.52	11.52	0.47
$^{19}F_{1.554}(3/2^+) + {}^{75}As_{0.280}(5/2^-)$	78.52	185.20	39.12
$^{19}F_{1.554}(3/2^+) + {}^{75}As_{0.304}(9/2^+)$	9.30	17.94	33.46
$^{19}F_{1.346}(5/2^-) + {}^{75}As_{0.572}(5/2^-)$		0.02	
$^{19}F_{1.459}(3/2^-) + {}^{75}As_{0.469}(1/2^-)$	0.04	0.04	<0.01
$^{19}F_{1.346}(5/2^-) + {}^{75}As_{0.618}(3/2^-)$		0.08	
$^{19}F_{1.554}(3/2^+) + {}^{75}As_{0.469}(1/2^-)$	128.55	141.49	1.99
$^{19}F_{1.459}(3/2^-) + {}^{75}As_{0.572}(5/2^-)$	<0.01	<0.01	<0.01
$^{19}F_{1.459}(3/2^-) + {}^{75}As_{0.618}(3/2^-)$	<0.01	0.04	<0.01
$^{19}F_{1.554}(3/2^+) + {}^{75}As_{0.572}(5/2^-)$	4.91	7.06	0.02
$^{19}F_{1.346}(5/2^-) + {}^{75}As_{0.822}(7/2^-)$		0.03	
$^{19}F_{1.554}(3/2^+) + {}^{75}As_{0.618}(3/2^-)$	3.80	60.82	0.26

experimental cross section is well reproduced considering all the adopted theoretical approaches (DWBA, CCBA and CRC), in particular at angles larger than $\theta_{c.m.} > 7°$.

The dominant contributions in ROI 2 [Fig. 6(b)] are given by the transitions to the $^{19}F_{0.197\ MeV}$ in connection with the two $3/2^-$ states of ^{75}As at $E_x = 0.618$ MeV and $E_x = 1.074$ MeV; the $^{19}F_{1.554\ MeV}$ state in connection with the ^{75}As ground state, the first $5/2^-$ state at $E_x = 0.280$ MeV, and the second $1/2^-$ state at $E_x = 0.469$ MeV. These last three states of ^{75}As are those contributing the most for ROI 1. In the ROI 2 case, although the inclusion of the coupled channels improves the agreement with data, the experimental cross section remains slightly underestimated. A possible explanation is that, due to the high level density of the residual nucleus, contributions from ^{75}As states at higher excitation energy were included in ROI 2. Further investigations of the cross section spectrum at higher excitation energies are ongoing and could significantly overcome the small difference between theory and experiment in ROI 2.

The agreement between theory and experiment found in this work for the $^{76}Se(^{18}O, ^{19}F)^{75}As$ reaction is consistent with the results recently obtained in the systematic exploration of one-nucleon transfer induced by the (^{18}O, ^{19}F) reaction on different targets [10,36,38]. These results point to remarkable control of the reaction mechanism and the interaction (*psd-mod*) chosen to describe the $\langle ^{19}F \,|\, ^{18}O\rangle$ projectile overlaps.

Exploratory calculations for $^{76}Se(^{18}O, ^{19}F)^{75}As$ one-proton pickup reaction were performed in order to confirm the sensitivity to different nuclear structure models when the reaction mechanism is set. In fact, in the case of the one-neutron stripping reaction induced by the $^{18}O + {}^{76}Se$ collision [37] we found that the experimental cross sections show an interesting sensitivity to the details of the adopted nuclear structure model.

For the sake of this nuclear structure model comparison, we calculated the DWBA cross sections by using spectroscopic amplitudes from IBFM for the target and shell-model for the projectile. The spectroscopic amplitudes (listed in Table IV) were calculated assuming configuration with a 0^+ boson coupled to a single proton in the same four orbitals ($0f_{5/2}$, $1p_{3/2}$, $1p_{1/2}$, and $0g_{9/2}$) adopted in the shell-model calculations. We did not perform CCBA calculations with the IBFM because

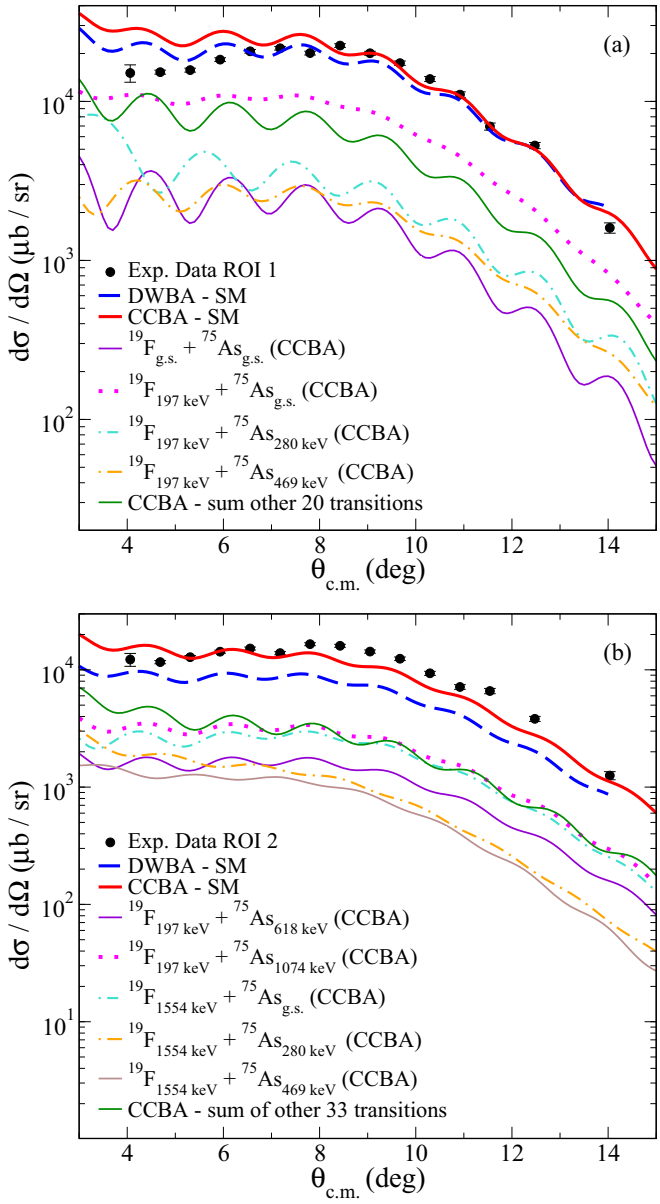

FIG. 6. Comparison between the theoretical and experimental cross sections for one-proton transfer angular distribution related to the contribution of the unresolved excited states of the ROIs 1 (a) and 2 (b). Most relevant transitions are shown together with the sum of all the contributing transitions for DWBA and CCBA calculations (see text).

IBM-2 does not predict a 2^+ state in the first low-lying excited states of ^{76}Se.

The experimental cross section is underestimated by the IBFM calculations in both ROI 1 and ROI 2, as is evident in Fig. 4. Comparing the shell-model and IBFM spectroscopic amplitudes (Table IV), the differences between the corresponding results can be unfolded. In general, shell-model spectroscopic amplitudes are larger respect to IBFM ones. In addition, it seems that shell-model distributes the strength among all the ^{75}As states with the same spin-parity, whereas IBFM model almost entirely attributes the strength to the first state. This behavior could be related to the fact that ^{75}As is built by coupling one proton to the core ^{74}Ge and not removing a proton from ^{76}Se.

V. CONCLUSIONS

In the present work, the ^{76}Se(^{18}O, ^{19}F)^{75}As one-proton pickup reaction at 275 MeV incident energy was studied for the first time. The experiment was performed at the INFN-LNS in Catania in the context of the NUMEN and NURE projects.

Excitation energy spectra and cross section angular distributions for transitions to the ground and low-lying excited states were extracted. Despite the good energy resolution, it was not possible to isolate transitions to individual states due to the high level density of the residual odd nucleus. In the context of the ongoing upgrade of the INFN-LNS facility [111], G-NUMEN, an array of 110 LaBr3(Ce) scintillators, will be installed around the object point of the MAGNEX magnetic spectrometer to detect the gamma rays emitted from the deexcitation of the excited states populated via DCE reactions with good energy resolution and detection efficiency, amidst a background composed of transitions from competing reaction channels with far higher cross sections [112,113]. Initial tests have been conducted on the first detectors of the array, allowing for the determination of their performance at high rates [114].

The experimental angular distributions for transitions to groups of states were compared to theoretical calculations based on DWBA, CCBA, and CRC approaches. According to the multichannel approach we sought for consistency with previous data analyses of scattering [46] and neutron transfer [37] reaction data. The optical potential for the initial partitions was chosen according to the elastic and inelastic scattering analysis of the ^{18}O + ^{76}Se collision [46]. The one-proton spectroscopic amplitudes for the projectile and target overlaps were derived by large-scale shell-model calculations using the same model space and interaction adopted in Ref. [37]. A remarkable agreement between theory and experiment both in cross section magnitude and diffraction pattern is obtained for the analyzed transitions, considering that no arbitrary scaling factors are used in the calculations. Moreover, a better agreement is obtained when inelastic excitations of projectile and target are included in the coupling scheme for the coupled-channels calculations, at least for the group of states lying at high excitation energies. On the other hand, considering the CRC approach with respect to the CCBA, the minor importance of the back-coupling of the transfer on the elastic channel is underlined.

The good description of the data through all the adopted theoretical approaches proves the validity of the nuclear structure and the adopted optical potentials. This result is very important for the NUMEN project and as a general finding for the analysis of direct nuclear reaction data for two reasons. First, it highlights that the multichannel approach guarantees an accurate investigation of all the interesting reactions induced by the ^{18}O + ^{76}Se collision. Second, we find that the mentioned couplings to inelastic states need to be investigated also for single and double charge exchange reactions.

Therefore, coupled-channels calculations are envisaged also for these reaction channels.

Exploratory calculations for ^{76}Se(^{18}O, ^{19}F)^{75}As reaction confirmed a remarkable sensitivity to different nuclear structure models, as already observed in ^{76}Se(^{18}O, ^{17}O)^{77}Se reaction. In this sense, heavy-ion nucleon transfer reactions can be probes to further constrain the many body states involved in the calculation of the nuclear matrix element (NME) of DCE and $0\nu\beta\beta$ processes.

A long term aim is to perform cross section calculations for one-nucleon transfer reactions from/to all the $0\nu\beta\beta$-candidates nuclei and compare them with the related experimental data from the NUMEN experiments. In this way, one can investigate if the adopted model spaces are reliable for the direct calculation of the NMEs.

ACKNOWLEDGMENTS

This project has received funding from the European Research Council (ERC) under the European Union's Horizon 2020 research and innovation program (Grant Agreement No. 714625). Support from the Brazilian funding agencies FAPESP Proc. No. 2019/07767-1, INCT-FNA Proc. No. 464898/2014-5, and CNPq Proc. No. 306353/2018-0, No. 408800/2021-6, and No. 301576/2022-0 is acknowledged. J.R.B.O. acknowledges a grant from CNPq Proc. No. 316019/2021-6. The Mexican authors acknowledge financial support from CONACyT 314857 and DGAPA-PAPIIT IG101423 and IG101120. We also acknowledge the CINECA award under the ISCRA initiative (code HP10BGLVFE) and through the INFN-CINECA agreement for the availability of high performance computing resources and support.

[1] H. Ejiri, J. Suhonen, and K. Zuber, Phys. Rep. **797**, 1 (2019).
[2] S. Dell'Oro, S. Marcocci, and F. Vissani, Phys. Rev. D **90**, 033005 (2014).
[3] M. J. Dolinski, A. W. Poon, and W. Rodejohann, Annu. Rev. Nucl. Part. Sci. **69**, 219 (2019).
[4] J. Engel and J. Menéndez, Rep. Prog. Phys. **80**, 046301 (2017).
[5] F. Cappuzzello, C. Agodi, M. Cavallaro *et al.*, Eur. Phys. J. A **54**, 72 (2018).
[6] F. Cappuzzello, M. Cavallaro, C. Agodi *et al.*, Eur. Phys. J. A **51**, 145 (2015).
[7] E. Santopinto, H. García-Tecocoatzi, R. I. Magaña-Vsevolodovna, and J. Ferretti, Phys. Rev. C **98**, 061601(R) (2018).
[8] H. Lenske, F. Cappuzzello, M. Cavallaro, and M. Colonna, Prog. Part. Nucl. Phys. **109**, 103716 (2019).
[9] J. Bellone *et al.*, Phys. Lett. B **807**, 135528 (2020).
[10] A. Spatafora, D. Carbone, F. Cappuzzello, M. Cavallaro, L. Acosta, C. Agodi, P. Amador-Valenzuela, T. Borello-Lewin, G. A. Brischetto, S. Calabrese, D. Calvo, V. Capirossi, E. R. Chávez Lomelí, I. Ciraldo, G. De Gregorio, F. Delaunay, H. Djapo, C. Eke, P. Finocchiaro, S. Firat *et al.* (NUMEN Collaboration), Phys. Rev. C **107**, 024605 (2023).
[11] S. Burrello, S. Calabrese *et al.*, Phys. Rev. C **105**, 024616 (2022).
[12] M. Cavallaro *et al.*, Front. Astron. Space Sci. **8**, 659815 (2021).
[13] F. Cappuzzello, H. Lenske, M. Cavallaro, C. Agodi, N. Auerbach, J. Bellone, R. Bijker, S. Burrello, S. Calabrese, D. Carbone, M. Colonna, G. De Gregorio, J. Ferreira, D. Gambacurta, H. García-Tecocoatzi, A. Gargano, J. Lay, R. Linares, J. Lubian, E. Santopinto *et al.*, Prog. Part. Nucl. Phys. **128**, 103999 (2023).
[14] J. L. Ferreira, J. Lubian, F. Cappuzzello, M. Cavallaro, and D. Carbone, Phys. Rev. C **105**, 014630 (2022).
[15] H. Lenske, H. H. Wolter, and H. G. Bohlen, Phys. Rev. Lett. **62**, 1457 (1989).
[16] S. Kahana and A. J. Baltz, *One- and Two-Nucleon Transfer Reactions with Heavy Ions*, edited by M. Baranger, E. Vogt, Advances in Nuclear Physics Vol. 9 (Springer, Boston, MA, 1977).
[17] N. Anyas-Weiss *et al.*, Phys. Rep. **12**, 201 (1974).
[18] H. Fulbright, C. L. Bennett, R. A. Lindgren, R. G.Markham, S. C. McGuire, G. C. Morrison, U. Strohbusch, and J. Toke, Nucl. Phys. A **284**, 329 (1977).
[19] W. Oelert, A. Djaloeis, C. Mayer-Böricke, P. Turek, and S. Wiktor, Nucl. Phys. A **306**, 1 (1978).
[20] W. Oertzen and A. Vitturi, Rep. Prog. Phys. **64**, 1247 (2001).
[21] D. Montanari, L. Corradi, S. Szilner, G. Pollarolo, E. Fioretto, G. Montagnoli, F. Scarlassara, A. M. Stefanini, S. Courtin, A. Goasduff, F. Haas, D. Jelavic Malenica, C. Michelagnoli, T. Mijatovic, N. Soic, C. A. Ur, and M. Varga Pajtler, Phys. Rev. Lett. **113**, 052501 (2014).
[22] A. Parmar, Sonika, B. J. Roy, V. Jha, U. K. Pal, T. Sinha, S. K. Pandit, V. V. Parkar, K. Ramachandran, K. Mahata *et al.*, Nucl. Phys. A **940**, 167 (2015).
[23] C. F. Maguire, G. L. Bomar, M. E. Barclay, R. B. Piercey, A. V. Ramayya, J. L. C. Ford, D. Shapira, E. R. Flynn, J. D. Moses, J. C. Peng, and N. Stein, Phys. Rev. Lett. **52**, 743 (1984).
[24] S. Szilner, L. Corradi, G. Pollarolo, S. Beghini, R. B. Behera, E. Fioretto, A. Gadea, F. Haas, A. Latina, G. Montagnoli, F. Scarlassara, A. M. Stefanini, M. Trotta, A. M. Vinodkumar, and Y. Wu, Phys. Rev. C **71**, 044610 (2005).
[25] D. K. Scott, P. N. Hudson, P. S. Fisher, C. U. Cardinal, N. Anyas-Weiss, A. D. Panagiotou, P. J. Ellis, and B. Buck, Phys. Rev. Lett. **28**, 1659 (1972).
[26] M. Cavallaro *et al.*, Phys. Rev. C **88**, 054601 (2013).
[27] M. J. Ermamatov *et al.*, Phys. Rev. C **94**, 024610 (2016).
[28] D. Carbone *et al.*, Phys. Rev. C **95**, 034603 (2017).
[29] R. Linares *et al.*, Phys. Rev. C **98**, 054615 (2018).
[30] E. N. Cardozo *et al.*, Phys. Rev. C **97**, 064611 (2018).
[31] J. L. Ferreira *et al.*, Phys. Rev. C **103**, 054604 (2021).
[32] F. Cappuzzello, D. Carbone, M. Cavallaro, M. Bondì, C. Agodi, F. Azaiez, A. Bonaccorso, A. Cunsolo, L. Fortunato, A. Foti *et al.*, Nat. Commun. **6**, 6743 (2015).
[33] M. Cavallaro, F. Cappuzzello, D. Carbone, and C. Agodi, Eur. Phys. J. A **55**, 244 (2019).
[34] D. Carbone *et al.*, Phys. Rev. C **102**, 044606 (2020).
[35] B. Paes, G. Santagati, R. I. Magaña-Vsevolodovna, F. Cappuzzello, D. Carbone, E. N. Cardozo, M. Cavallaro, H. Garcia-Tecocoatzi, A. Gargano, J. L. Ferreira, S. M. Lenzi, R.

Linares, E. Santopinto, A. Vitturi, and J. Lubian, Phys. Rev. C **96**, 044612 (2017).
[36] S. Calabrese *et al.*, Phys. Rev. C **104**, 064609 (2021).
[37] I. Ciraldo *et al.*, Phys. Rev. C **105**, 044607 (2022).
[38] O. Sgouros *et al.*, Phys. Rev. C **104**, 034617 (2021).
[39] O. Sgouros, M. Cutuli, F. Cappuzzello, M. Cavallaro, D. Carbone, C. Agodi, G. De Gregorio, A. Gargano, R. Linares, G. A. Brischetto, D. Calvo, E. R. Chávez Lomelí, I. Ciraldo, F. Delaunay, H. Djapo, C. Eke, P. Finocchiaro, M. Fisichella, M. A. Guazzelli, A. Hacisalihoglu *et al.* (for the NUMEN Collaboration), Phys. Rev. C **108**, 044611 (2023).
[40] F. Cappuzzello, C. Agodi, D. Carbone, and M. Cavallaro, Eur. Phys. J. A **52**, 169 (2016).
[41] F. Cappuzzello, D. Carbone, M. Cavallaro, and A. Cunsolo, *Magnets: Types, Uses and Safety*, Materials Science and Technologies Series Vol. 52 (Nova Science, New York, 2011).
[42] F. Cappuzzello *et al.*, Phys. Lett. B **711**, 347 (2012).
[43] A. Bonaccorso, F. Cappuzzello, D. Carbone, M. Cavallaro, G. Hupin, P. Navratil, and S. Quaglioni, Phys. Rev. C **100**, 024617 (2019).
[44] D. Carbone, Eur. Phys. J. Plus **130**, 143 (2015).
[45] M. J. Ermamatov *et al.*, Phys. Rev. C **96**, 044603 (2017).
[46] L. La Fauci, A. Spatafora, F. Cappuzzello, C. Agodi, D. Carbone, M. Cavallaro, J. Lubian, L. Acosta, P. Amador-Valenzuela, T. Borello-Lewin, G. A. Brischetto, S. Calabrese, D. Calvo, V. Capirossi, E. R. Chavez Lomeli, I. Ciraldo, M. Cutuli, F. Delaunay, H. Djapo, C. Eke *et al.*, Phys. Rev. C **104**, 054610 (2021).
[47] N. Keeley, K. W. Kemper, and K. Rusek, Phys. Rev. C **106**, 014623 (2022).
[48] F. Wamers, C. Lehr, J. Marganiec-Gałazka, F. Aksouh, Yu. Aksyutina, H. Alvarez-Pol, L. Atar, T. Aumann, S. Beceiro-Novo, C. A. Bertulani, K. Boretzky, M. J. G. Borge, C. Caesar, M. Chartier, A. Chatillon, L. V. Chulkov, D. Cortina-Gil, P. Díaz Fernández, H. Emling, O. Ershova *et al.*, Eur. Phys. J. A **59**, 154 (2023);
[49] T. Pohl, Y. L. Sun, A. Obertelli, J. Lee, M. Gómez-Ramos, K. Ogata, K. Yoshida, B. S. Cai, C. X. Yuan, B. A. Brown, H. Baba, D. Beaumel, A. Corsi, J. Gao, J. Gibelin, A. Gillibert, K. I. Hahn, T. Isobe, D. Kim, Y. Kondo *et al.*, Phys. Rev. Lett. **130**, 172501 (2023).
[50] M. Cavallaro *et al.*, PoS **BORMIO2017**, 015 (2017).
[51] D. Torresi *et al.*, Nucl. Instrum. Methods Phys. Res., Sect. A **989**, 164918 (2021).
[52] F. Cappuzzello *et al.*, Nucl. Instrum. Methods Phys. Res., Sect. A **621**, 419 (2010).
[53] S. Calabrese *et al.*, Nucl. Instrum. Methods Phys. Res., Sect. A **980**, 164500 (2020).
[54] G. Souliotis *et al.*, Nucl. Instrum. Methods Phys. Res., Sect. A **1031**, 166588 (2022).
[55] S. Koulouris, G. A. Souliotis, F. Cappuzzello, D. Carbone, A. Pakou, C. Agodi, G. A. Brischetto, S. Calabrese, M. Cavallaro, I. Ciraldo, O. Fasoula, J. Klimo, O. Sgouros, V. Soukeras, A. Spatafora, D. Torresi, and M. Veselsky, Phys. Rev. C **108**, 044612 (2023).
[56] F. Cappuzzello, D. Carbone, and M. Cavallaro, Nucl. Instrum. Methods Phys. Res., Sect. A **638**, 74 (2011).
[57] F. Cappuzzello, C. Agodi, M. Bondì, D. Carbone, M. Cavallaro, A. Cunsolo, M. D. Napoli, A. Foti, and D. Nicolosi, Nucl. Instrum. Methods Phys. Res., Sect. A **763**, 314 (2014).
[58] M. Cavallaro, F. Cappuzzello, D. Carbone, A. Cunsolo, A. Foti, and R. Linares, Nucl. Instrum. Methods Phys. Res., Sect. A **637**, 77 (2011).
[59] I. Ciraldo, Nuovo Cimento C **44**, 38 (2021).
[60] D. M. Brink, Phys. Lett. B **40**, 37 (1972).
[61] R. Bass, *Nuclear Reactions with Heavy Ions*, Theoretical and Mathematical Physics (Springer, Berlin, 1980).
[62] N. Shimizu, T. Mizusaki, T. Utsuno, and Y. Tsunoda, Comput. Phys. Commun. **244**, 372 (2019).
[63] Y. Utsuno and S. Chiba, Phys. Rev. C **83**, 021301(R) (2011).
[64] E. K. Warburton and B. A. Brown, Phys. Rev. C **46**, 923 (1992).
[65] C. Schmidt and H. Duhm, Nucl. Phys. A **155**, 644 (1970).
[66] L. Green, C. Lennon, and I. Naqib, Nucl. Phys. A **142**, 137 (1970).
[67] M. Yasue, T. Hasegawa, S. I. Hayakawa, K. Ieki, J. Kasagi, S. Kubono, T. Murakami, K. Nisimura, K. Ogawa, H. Ohnuma, R. J. Peterson, H. Shimizu, M. H. Tanaka, and H. Toyokawa, Phys. Rev. C **46**, 1242 (1992).
[68] V. Burjan, Z. Hons, V. Kroha, J. Mrázek, Š. Piskoř, A. Mukhamedzhanov, L. Trache, R. Tribble, M. La Cognata, L. Lamia *et al.*, Eur. Phys. J. A **55**, 114 (2019).
[69] M. B. Tsang, J. Lee, and W. G. Lynch, Phys. Rev. Lett. **95**, 222501 (2005).
[70] L. Coraggio, L. De Angelis, T. Fukui, A. Gargano, N. Itaco, and F. Nowacki, Phys. Rev. C **100**, 014316 (2019).
[71] M. Rocchini *et al.*, Phys. Rev. C **103**, 014311 (2021).
[72] R. Machleidt, Phys. Rev. C **63**, 024001 (2001).
[73] S. Bonger, T. T. S. Kuo, and L. Coraggio, Nucl. Phys. A **684**, 432 (2001).
[74] L. Coraggio, A. Covello, A. Gargano *et al.*, Ann. Phys. **327**, 2125 (2012).
[75] NNDC, data extracted using the NNDC On-Line Data Service from the ENSDF database, http://www.nndc.bnl.gov/ensdf/.
[76] D. Rudolph, D. Weisshaar, F. Cristancho, J. Eberth, C. Fahlander, O. Iordanov, S. Skoda, C. Teich, O. Thelen, and H. Thomas, Eur. Phys. J. A **6**, 377 (1999).
[77] R. M. Pérez-Vidal, A. Gadea, C. Domingo-Pardo, A. Gargano, J. J. Valiente-Dobón, E. Clément, A. Lemasson, L. Coraggio, M. Siciliano, S. Szilner, M. Bast, T. Braunroth, J. Collado, A. Corina, A. Dewald, M. Doncel, J. Dudouet, G. de France, C. Fransen, V. González *et al.*, Phys. Rev. Lett. **129**, 112501 (2022).
[78] A. Juodagalvis and S. Åberg, Nucl. Phys. A **683**, 207 (2001).
[79] M. Hasegawa, K. Kaneko, and T. Mizusaki, Phys. Rev. C **71**, 044301 (2005).
[80] M. Hasegawa, K. Kaneko, and T. Mizusaki, Phys. Rev. C **72**, 064320 (2005).
[81] G. Rotbard, M. Vergnes, J. Vernotte, G. Berrier-Ronsin, J. Kalifa, and R. Tamisier, Nucl. Phys. A **401**, 41 (1983).
[82] B. P. Kay, J. P. Schiffer, S. J. Freeman, T. Adachi, J. A. Clark, C. M. Deibel, H. Fujita, Y. Fujita, P. Grabmayr, K. Hatanaka, D. Ishikawa, H. Matsubara, Y. Meada, H. Okamura, K. E. Rehm, Y. Sakemi, Y. Shimizu, H. Shimoda, K. Suda, Y. Tameshige *et al.* (private communication).
[83] L. Coraggio, G. De Gregorio, A. Gargano, N. Itaco, T. Fukui, Y. Z. Ma, and F. R. Xu, Phys. Rev. C **102**, 054326 (2020).
[84] L. Coraggio, G. DeGregorio, A. Gargano, N. Itaco, T. Fukui, Y. Z. Ma, and F. R. Xu, Phys. Rev. C **104**, 054304 (2021).
[85] I. Ciraldo *et al.*, J. Phys. Conf. Ser. **2453**, 012013 (2023).
[86] F. Iachello and A. Arima, Adv. Nucl. Phys., 139 (1984).

[87] F. Iachello and P. V. Isacker, *The Interacting Boson-Fermion Model*, Cambridge Monographs on Mathematical Physics (Cambridge University Press, Cambridge, 1991).
[88] J. Ferretti, J. Kotila, R. I. Magaña-Vsevolodovna, and E. Santopinto, Phys. Rev. C **102**, 054329 (2020).
[89] J. Bardeen, L. N. Cooper, and J. R. Schrieffer, Phys. Rev. **108**, 1175 (1957).
[90] C. E. Alonso, J. M. Arias, R. Bijker, and F. Iachello, Phys. Lett. B **144**, 141 (1984).
[91] J. M. Arias, Ph.D. dissertation, University of Sevilla, 1985 (unpublished).
[92] C. E. Alonso, Ph.D. dissertation, University of Sevilla, 1986 (unpublished).
[93] J. M. Aria, C. E. Alonso, and R. Bijker, Nucl. Phys. A **445**, 333 (1985).
[94] J. Barea, J. Kotila, and F. Iachello, Phys. Rev. C **87**, 014315 (2013).
[95] I. J. Thompson, Phys. Rep. **7**, 167 (1988).
[96] I. Thompson and F. Nunes, *Nuclear Reactions for Astrophysics: Principles, Calculation and Applications of Low-Energy Reactions*, 1st ed. (Cambridge University Press, Cambridge, 2009).
[97] L. C. Chamon, B. V. Carlson, L. R. Gasques, D. Pereira, C. De Conti, M. A. G. Alvarez, M. S. Hussein, M. A. Cândido Ribeiro, E. S. Rossi, and C. P. Silva, Phys. Rev. C **66**, 014610 (2002).
[98] M. A. G. Alvarez *et al.*, Nucl. Phys. A **723**, 93 (2003).
[99] L. R. Gasques, L. C. Chamon, P. R. S. Gomes, and J. Lubian, Nucl. Phys. A **764**, 135 (2006).
[100] D. P. Sousa, D. Pereira, J. Lubian, L. C. Chamon, J. R. B. Oliveira, E. S. Rossi, Jr., C. P. Silva, P. N. de Faria, V. Guimarães, R. Lichtenthaler, and M. A. G. Alvarez, Nucl. Phys. A **836**, 1 (2010).
[101] D. Pereira, J. Lubian, J. R. B. Oliveira, D. P. de Souza, and L. C. Chamon, Phys. Lett. B **670**, 330 (2009).
[102] D. Carbone *et al.*, Universe **7**, 58 (2021).
[103] A. Spatafora *et al.*, Phys. Rev. C **100**, 034620 (2019).
[104] V. Zagatto *et al.*, Phys. Rev. C **97**, 054608 (2018).
[105] J. R. B. Oliveira *et al.*, J. Phys. G: Nucl. Part. Phys. **40**, 105101 (2013).
[106] D. Pereira *et al.*, Phys. Lett. B **710**, 426 (2012).
[107] G. Brischetto *et al.*, Phys. Rev. C **109**, 014604 (2023).
[108] B. Pritychenko, M. Birch, B. Singh, and M. Horoi, At. Data Nucl. Data Tables **107**, 1 (2016).
[109] T. Kibédi and R. Spear, At. Data Nucl. Data Tables **80**, 35 (2002).
[110] K. Suzuki and R. Okamoto, Prog. Theor. Phys. **93**, 905 (1995).
[111] F. Cappuzzello *et al.*, Int. J. Mod. Phys. A **36**, 2130018 (2021).
[112] P. Finocchiaro *et al.*, Universe **6**, 129 (2020).
[113] J. Oliveira, P. Finocchiaro, C. Agodi, I. Boztosun, F. Cappuzzello, P. De Faria, L. Gasques, R. Linares, N. Medina, D. Mendes *et al.*, J. Phys. Conf. Ser. **1056**, 012040 (2018).
[114] E. M. Gandolfo, J. R. B. Oliveira, L. Campajola, D. Pierroutsakou, A. Boiano, C. Agodi, F. Cappuzzello, D. Carbone, M. Cavallaro, I. Ciraldo, D. Calvo, F. Delaunay, C. Eke, F. Longhitano, N. Medina, M. Moralles, D. Sartirana, V. R. Sharma, A. Spatafora, D. Toufen *et al.*, Instruments **7**, 28 (2023).